



# A numerical investigation of the prompt oblique detonation wave sustained by a finite-length wedge

Yan Liu<sup>1</sup> · Xudong Han<sup>1</sup> · Songbai Yao<sup>1</sup> · Jianping Wang<sup>1</sup>

Received: 31 August 2015 / Revised: 28 January 2016 / Accepted: 5 February 2016 / Published online: 2 March 2016  
© Springer-Verlag Berlin Heidelberg 2016

**Abstract** The prompt oblique detonation wave (PODW) sustained by a finite-length wedge is investigated by numerical simulation. The numerical results show that it is possible to stabilize a PODW on a finite-length wedge shorter than the induction length of the mixture behind the inert shock by numerically imposing a premature initiation of combustion in the initial flow field. The fully coupled and the partially coupled PODWs are observed in the numerical results. For the fully coupled PODW, the upstream facing transverse waves (UF TW) are swept downstream and consequently a fully coupled PODW can persist. For the partially coupled PODW, the UF TWs propagate upstream and the downstream facing transverse waves are weakened by the expansion wave emanating from the corner. As a result, a partially coupled PODW forms. Further, it is found that the stability of the partially coupled PODW is weak. The configuration of the partially coupled PODW can be altered by local explosions occurring downstream.

**Keywords** Oblique detonation wave · Transverse wave · Expansion wave

Communicated by A. Higgins.

✉ Yan Liu  
liuyandeyoux@126.com  
Xudong Han  
1400737965@qq.com  
Songbai Yao  
yaos@pku.edu.cn  
Jianping Wang  
wangjp@pku.edu.cn

<sup>1</sup> Center for Combustion and Propulsion, CAPT and SKLTCS, Department of Mechanics and Engineering Science, College of Engineering, Peking University, Beijing 100871, China

## 1 Introduction

An oblique detonation wave (ODW) is a detonation wave that is stabilized on an obstacle in supersonic flows of detonable mixtures. ODWs are regarded as a potential combustion mechanism for supersonic propulsion systems, such as the ODW engine [1] or the ram accelerator [2]. ODWs received considerable attention in previous decades, and extensive work on ODWs [3–22] has been done in earlier research.

Generally, the ODW can be divided into two kinds, the delayed ODW [3,4] and the prompt ODW [4–6] (PODW). Figure 1 presents schematics of these two kinds of ODWs. As shown in Fig. 1a, the delayed ODW transitions from an oblique shock wave (OSW). As shown in Fig. 1b, the PODW directly forms at the wedge tip without an obvious transition process. According to Li et al. [7], the structure of the delayed ODW consists of an oblique non-reactive shock wave (OSW), an induction region, a set of deflagration waves, and an oblique reactive shock wave, namely the ODW front. By numerical simulation, Liu et al. [8] found that the structure of the delayed ODW changed as the inflow Mach number increased. Two kinds of OSW–ODW transition were observed in the numerical results of Figueira da Silva and Deshaies [3], namely the smooth transition and the abrupt transition. By numerical simulation, Papalexandris [9] found that the smooth OSW–ODW transition was likely to occur at small wedge angles, while the abrupt OSW–ODW transition was likely to occur at large wedge angles. Teng and Jiang [10] used the angle difference between the OSW and the ODW as the criterion to determine the transition pattern. It was found that the smooth OSW–ODW transition would appear when the angle difference was small, while the abrupt transition would occur when the angle difference was large.

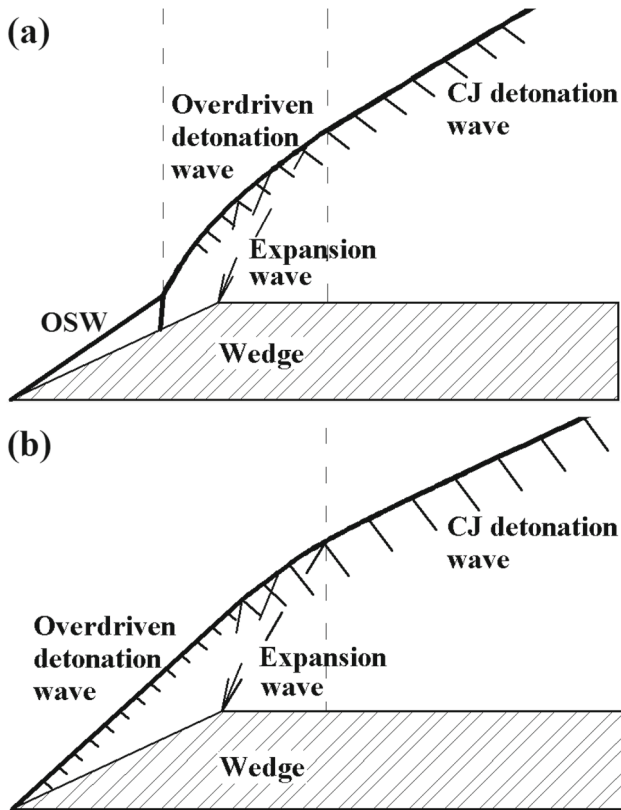


**Fig. 1** Schematics of **a** the delayed ODW and **b** the PODW

By numerical simulation, Teng et al. [11] found that the instability of the ODW front could appear even at a high degree of overdrive, up to 2.37. According to Choi et al. [12], the ODW front was likely to become unstable and form cell-like structures at high activation energy. According to the numerical results of Teng et al. [13], the upstream facing transverse wave (UF TW) formed earlier than the downstream facing transverse wave (DF TW). Their numerical results indicated that high activation energy and low wedge angle were beneficial to the UF TW formation. Verreault et al. [14] verified that the spatial oscillation of the oblique shock wave was the origin of the UF TWs, and the temporal instability of the spatial oscillation was the origin of the DF TWs. Based on the stability of the ODW front, Gui et al. [15] divided it into three sections, i.e., the Zeldovich–von Neumann–Döring (ZND) model-like structure, single-sided triple point structure, and dual-headed triple point structure.

In the experiments of Verreault and Higgins [4], two kinds of PODW were observed. The PODW at high initial pressure weakened to a Chapman–Jouguet (CJ) ODW, while the PODW at low initial pressure decoupled. According to the numerical simulations of Papalexandris [9], Walter et al. [16], and Pimentel et al. [17], the weakening effect of the expansion wave (EW) emanating from the corner was the reason why

the PODW decoupled or weakened to a CJ ODW. By numerical simulation, Lefebvre and Fujiwara [5] and Liu et al. [6] found that the PODW was likely to occur at low inflow Mach number and high wedge angle. In the experiments of Kasahara et al. [18–21], the decoupled PODW was observed to be followed by another ODW, and they named this wave configuration the straw-hat type. In the experimental results of Maeda et al. [22], the second ODW of the straw-hat type configuration was observed to be convected downstream.

According to Verreault and Higgins [4] and Papalexandris [9], to initiate an ODW, the wedge length should not be shorter than the length of the induction region. Otherwise, even if the reaction process is initiated by the initial conditions, the reacted material will be convected downstream. Consequently, the ODW cannot occur. Essentially, the PODW is an oblique shock wave that couples with a reaction front. The detonation products flow away from the PODW at supersonic velocity. Furthermore, the length of the induction region of the PODW  $l_{\text{num,ind}}$  is always much shorter than the induction length determined by the post-shock state of the OSW  $l_{\text{p-s,ind}}$  [6]. Therefore, theoretically, the length of the wedge used to initiate a PODW is not limited by  $l_{\text{p-s,ind}}$ . This is a very desirable feature for propulsion applications. However, the initiation and stabilization process of the PODW is unclear when the wedge length is shorter than  $l_{\text{p-s,ind}}$ .

In this study, the influence of the initial condition on the initiation and stabilization of the PODW is investigated by numerical simulation. Further, the sustaining mechanism of the stabilized PODW is studied. In the numerical simulation, a two-step chemical reaction model proposed by Korobeinikov et al. [23] is adopted. With this reaction model, the value of heat release is determined by the post-shock state of the ODW instead of a constant. This is a desirable feature in the simulation of the ODW that often deviates from the CJ state. Because of its simplicity, it allows us to simulate the ODW with a high-resolution algorithm and small grid size. Moreover, it can reproduce correct ODW structures that qualitatively agree with the previous experimental [18–22] and numerical [16, 17] results. This is another reason we chose this chemical reaction model.

## 2 Physical model and numerical method

In this study, viscosity, thermal conduction, and mass diffusion of the mixtures are neglected. The two-dimensional Euler equations in generalized coordinates coupled with a two-step chemical reaction model [23] are solved. The governing equations are summarized as follows

$$\frac{\partial \mathbf{U}}{\partial t} + \frac{\partial \mathbf{E}}{\partial \xi} + \frac{\partial \mathbf{F}}{\partial \eta} = \mathbf{S} \quad (1)$$

$$\begin{aligned} \mathbf{U} &= J^{-1} \begin{bmatrix} \rho \\ \rho u \\ \rho v \\ e \\ \rho\alpha \\ \rho\beta \end{bmatrix}, \quad \mathbf{E} = J^{-1} \begin{bmatrix} \rho U \\ \rho u U + \xi_x p \\ \rho v U + \xi_y p \\ (e + p)U \\ \rho\alpha U \\ \rho\beta U \end{bmatrix}, \\ \mathbf{F} &= J^{-1} \begin{bmatrix} \rho V \\ \rho u V + \eta_x p \\ \rho v V + \eta_y p \\ (e + p)V \\ \rho\alpha V \\ \rho\beta V \end{bmatrix}, \quad \mathbf{S} = J^{-1} \begin{bmatrix} 0 \\ 0 \\ 0 \\ 0 \\ \rho\omega_\alpha \\ \rho\omega_\beta \end{bmatrix} \quad (2) \\ J &= \begin{vmatrix} \xi_x & \xi_y \\ \eta_x & \eta_y \end{vmatrix}, \quad \xi_x = J y_\eta, \quad \xi_y = -J x_\eta, \\ \eta_x &= -J y_\xi, \quad \eta_y = J x_\xi \quad (3) \\ U &= \xi_x u + \xi_y v, \quad V = \eta_x u + \eta_y v \quad (4) \end{aligned}$$

Here  $\rho$  is the density,  $p$  the pressure,  $u$  the velocity component along the physical coordinate  $x$ -axis, and  $v$  the velocity component along the physical coordinate  $y$ -axis.  $e$  is the total energy per unit volume, which is given by the following expression

$$e = \frac{p}{\gamma - 1} + \beta\rho q + \frac{1}{2}\rho(u^2 + v^2) \quad (5)$$

$\alpha$  is the progress variable of induction reaction which decreases from unity.  $\beta$  is the progress variable of exothermic reaction which decreases from unity when  $\alpha$  goes below zero. The chemical reaction rates are given by the following expressions

$$\omega_\alpha = \frac{d\alpha}{dt} = -k_1\rho \exp(-E_1/RT) \quad (6)$$

$$\omega_\beta = \frac{d\beta}{dt} = \begin{cases} -k_2 p^2 \left[ \beta^2 \exp\left(\frac{-E_2}{RT}\right) \right. \\ \left. -(1-\beta)^2 \exp\left(-\frac{E_2+q}{RT}\right) \right] & (\alpha \leq 0) \\ 0 & (0 < \alpha \leq 1) \end{cases} \quad (7)$$

The mixture adopted in this study is stoichiometric hydrogen-air. The temperature and pressure of the incoming mixture are fixed at 300 K and 1 atm. The parameters of the reaction model are listed in Table 1. They are the same with those of Liu [24] for stoichiometric hydrogen-air.

The Steger-Warming approach [25] is adopted to split the flux vectors, and the 5th order weighted essentially non-oscillatory (WENO) scheme [26] is used to integrate the split flux vectors. Figure 2 shows a schematic of the computational domain which is surrounded by dashed lines. The

**Table 1** Parameters of the reaction model

Model parameters	Value
$q$	$2.4 \times 10^6 \text{ J/kg}$
$R$	$3.978 \times 10^2 \text{ J/kg/K}$
$k_1$	$1.8 \times 10^8 \text{ m}^3/\text{kg/s}$
$k_2$	$0.5 \times 10^{-5} \text{ m}^4/\text{N}^2/\text{s}$
$E_1/R$	9800 K
$E_2/R$	2000 K

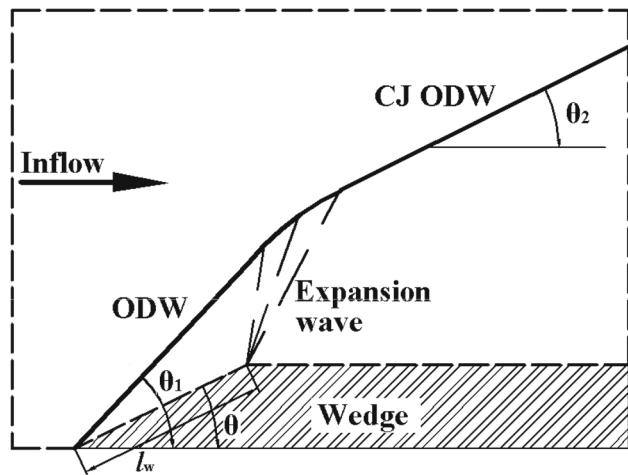


**Fig. 2** Schematic of the computational domain.  $l_w$ —wedge length;  $\theta_1$ —angle of the ODW above the wedge;  $\theta_2$ —angle of the CJ ODW

upper boundary of the computational domain is set beyond the extent of the ODW. The grid size  $\Delta x$  along the  $x$ -axis is fixed at 0.02 mm. In the  $y$ -direction, the grids are averagely distributed along the  $y$ -axis, and the grid size is always kept smaller than 0.02 mm. With these grid sizes, about 7 cells will be situated in the induction zone of the overdriven ODW at an inflow Mach number  $M = 7.0$  and wedge angle  $\theta = 27^\circ$ .

The hydrogen-air mixtures flow into the computational domain through the left boundary, and flow out through the right boundary. Therefore, the boundary conditions at the left and upper boundaries are fixed at the initial values. A slip boundary condition is used at the wedge surface and wedge shoulder. The zero-gradient condition is imposed to the right boundary and the first part of the bottom boundary.

### 3 Results and discussion

#### 3.1 PODW induced by an infinite-length wedge

All the calculation conditions are summarized in Table 2. In all the cases, the wedge angle is fixed at  $27^\circ$ . As a basis, the PODW induced by an infinite-length wedge is first introduced. The initiation process and stabilization process of the PODW have been presented by Lefebvre and Fujiwara [5]

**Table 2** Summary of calculations

Case	$M$	$l_w$ (mm)	State <sup>a</sup>
1	7.0	Infinite	F
2	6.5	Infinite	F
3	7.0	5	F
4	6.5	9	P
5	6.5	7	P
6	6.5	5	P

<sup>a</sup> F fully coupled PODW, P partially coupled PODW

and Liu et al. [6]. For clarity, the process which results in a PODW is briefly recalled hereafter. Figure 3 shows the initiation process and stabilization process of the PODW induced by an infinite-length wedge at  $M = 7.0$  and  $\theta = 27^\circ$ , namely case 1 in Table 2. The OSW induced by the corresponding wedge is taken as the initial condition. The flow characteristics behind the OSW are post-shock pressure  $p_{p-s} = 19.5$  atm, post-shock temperature  $T_{p-s} = 1262.3$  K, and post-shock flow velocity  $u_{p-s} = 2346.7$  m/s. This leads to a value of  $l_{p-s,ind} = 8.17$  mm, where  $l_{p-s,ind} = u_{p-s} \times t_{p-s,ind}$ .  $t_{p-s,ind}$  is the induction time determined by the post-shock state of the OSW and calculated with Eq. 6.

As shown in Fig. 3a, the initiation of combustion occurs over the wedge surface and consequently a half-round pressure wave forms [6]. The distance between the wedge tip and the initiation location is about 8.2 mm, which compares well with the induction length  $l_{p-s,ind}$ , 8.17 mm. The coalescence of the half-round pressure wave and the OSW results in the formation of the ODW. As shown in Fig. 3b, c, the newly formed ODW propagates upstream and eventually stabilizes at the wedge tip. The length of the induction region  $l_{num,ind}$  in Fig. 3c is about 1.4 mm, which is much smaller than  $l_{p-s,ind}$ , 8.17 mm. The shorter length of the induction region is a typical characteristic of the PODW. With the flow field at

$M = 7.0$  shown in Fig. 3c as the initial condition, the ODW at  $M = 6.5$  is obtained by numerical simulation. The ODW at  $M = 6.5$  turns out to be a PODW as well. This is consistent with the tendency presented in Refs. [5, 6] that the decrease of inflow Mach number is conducive to the formation of the PODW.

The angle of the stabilized PODW shown in Fig. 3c is about  $53^\circ$ , which is in good agreement with the value,  $53.1^\circ$ , obtained by shock polar analysis. The corresponding normal Mach number of the PODW  $M_n$  is about 5.59. The CJ Mach number of stoichiometric hydrogen–air at 1 atm and 300 K  $M_{CJ}$  is about 4.84. Therefore, the PODW is overdriven. The degree of overdrive  $f$  is about 1.33, where  $f = (M_n/M_{CJ})^2$ . To test the mesh independence of the numerical results, the grid size was doubled and halved. Figure 4 shows the corresponding pressure fields. The angles of the stabilized PODWs are both fixed at  $53^\circ$ . The PODWs shown in Figs. 3c and 4b both contain 42 UF TWs. The change of the cellular structures with halved grid size is negligible relative to those observed in Fig. 3c. Therefore, it can be concluded that the grid size adopted in this study is acceptable.

### 3.2 PODW sustained by a finite-length wedge

#### 3.2.1 Initial conditions

To obtain the inert shock wave induced by a finite-length wedge, the numerical simulations were performed with the heat release reaction of the mixtures switched off. Figure 5 shows the distribution of the induction progress variable  $\alpha$  and the temperature contours at  $M = 7.0$  and wedge length  $l_w = 5$  mm. As observed in Fig. 5, the post-shock temperature above the wedge surface is uniform. The induction length  $l_{p-s,ind}$  determined by the flow state in this uniform region is about 8.17 mm, which is longer than  $l_w = 5$  mm. Therefore, the induction process cannot be completed in this

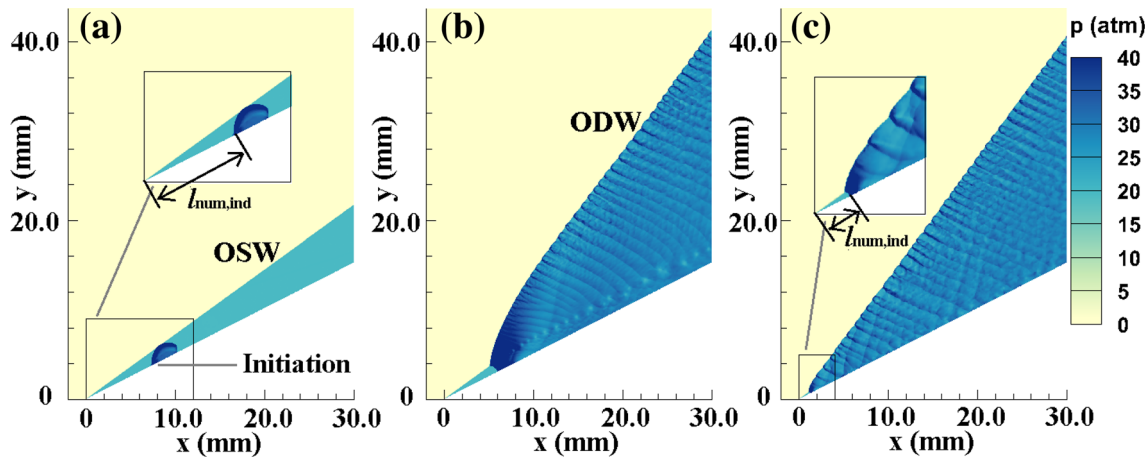


**Fig. 3** Pressure fields of the PODW at  $M = 7.0$  at different times

**Fig. 4** Pressure fields of the stabilized PODW at  $M = 7.0$  with the **a** doubled and **b** halved grid sizes

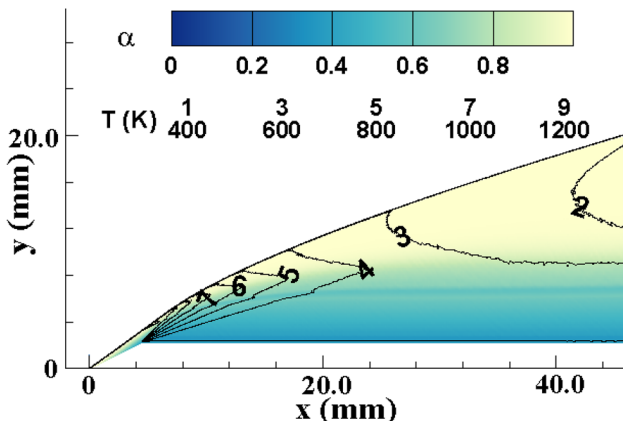
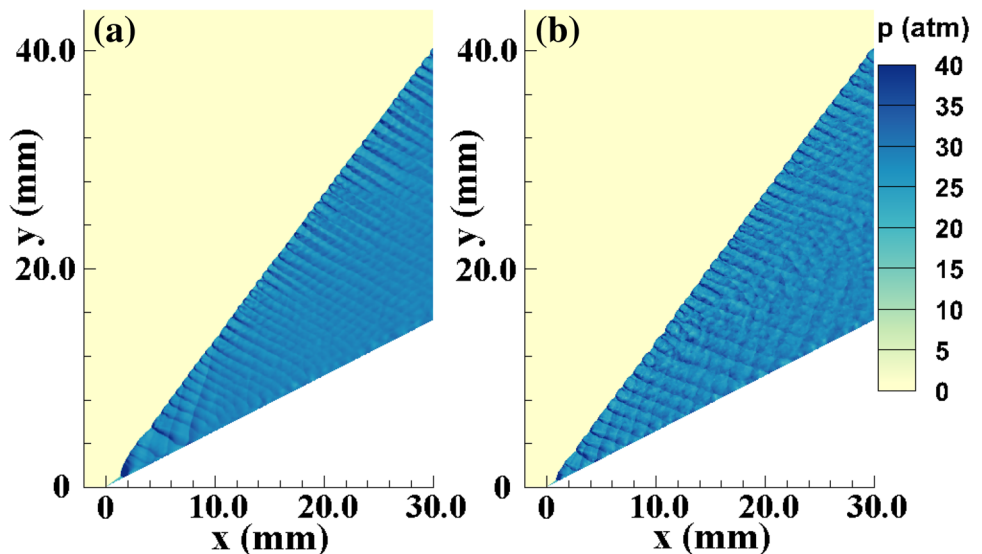


**Fig. 5** Distribution of the induction progress variable  $\alpha$  and the temperature contours behind the OSW at  $M = 7.0$  and  $l_w = 5$  mm

uniform region. As the mixture passes through the expansion wave (EW) emanating from the corner, its temperature decreases rapidly. As a result, the induction process is dramatically slowed down, and cannot be completed in the computational domain. Resulting from the low temperature, the induction reaction cannot be completed outside the computational domain as well. Therefore, an ODW would not occur if such an inert shock wave is taken as the initial condition. A similar phenomenon was also observed in the cases of  $M = 6.5$  and  $l_w = 5, 7$ , and  $9$  mm.

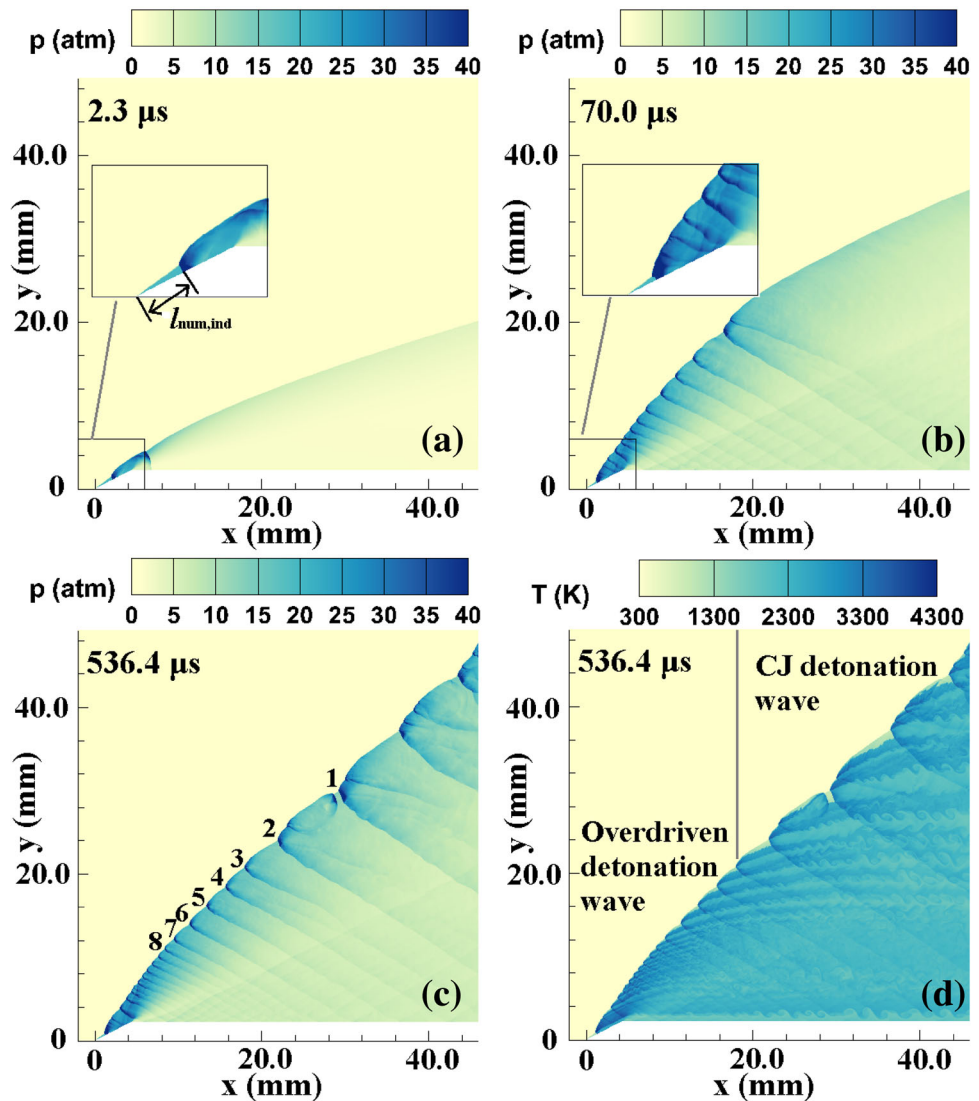
To initiate the ODW, a disturbance of partially induced hydrogen–air with  $\alpha = 0.2$  was introduced into the initial flow field. The size of the disturbance is  $2\text{ mm} \times 2\text{ mm}$ , and it is located in  $(x, y) \in [-2\text{ mm}, 0] \times [0, 2\text{ mm}]$ . As shown in the following sections, a PODW is successfully initiated with such a disturbance, and successfully sustained by a finite-length wedge.

### 3.2.2 Fully coupled PODW

Figure 6 shows the formation process of the PODW at  $M = 7.0$  and  $l_w = 5$  mm. Due to the above-mentioned disturbance, the premature initiation of combustion occurs above the wedge surface as shown in Fig. 6a. After the initiation, an ODW featured by TWs is formed in the flow field as shown in Fig. 6b. A comparison between Fig. 6a, b shows that the newly formed ODW propagates upstream. The lengths of the induction region  $l_{\text{num,ind}}$  in Fig. 6b, c are apparently smaller than that in Fig. 6a. Moreover, the value of  $l_{\text{num,ind}}$  of the stabilized ODW in Fig. 6c is about 1.4 mm, which compares well with the value obtained with an infinite-length wedge. This induction length of the stabilized ODW is much shorter than the induction length  $l_{\text{p-s,ind}}$ , 8.17 mm, determined by the post-shock state of the OSW. Therefore, similar to the ODW sustained by an infinite-length wedge, the ODW is a PODW as well in this case.

Essentially, the PODW over a wedge is an oblique shock wave that couples with a reaction front. The post-shock detonation products flow away from the PODW at supersonic velocity. Therefore, the PODW above the wedge is out of the influence of the EW emanating from the downstream corner. As a result, the angle of the PODW remains almost constant and is about  $53.5^\circ$ , which compares well with the value,  $53.1^\circ$ , obtained by shock polar analysis. The normal Mach number of the PODW  $M_n$  is about 5.63, which is greater than  $M_{\text{CJ}}$ , 4.84. The degree of overdrive of the PODW  $f$  is about 1.35. Resulting from the weakening effect of the EW, the PODW in the vicinity of the corner becomes weaker, and its angle decreases. Behind the EW, the angle of PODW remains almost constant and is about  $43^\circ$ . The corresponding normal Mach number of the PODW is about 4.77, which is in good agreement with  $M_{\text{CJ}}$ , 4.84. Therefore, the PODW behind the

**Fig. 6** Formation process of the PODW at  $M = 7.0$  and  $l_w = 5 \text{ mm}$



EW should be at the CJ state. A similar phenomenon has also been observed in the experiments of Verreault and Higgins [4] and Kasahara et al. [19, 20].

According to the shock polar analysis, the post-shock tangential Mach numbers of the PODW above the wedge and at the CJ state are 1.3 and 2.1, respectively. Further, because the TWs of detonation are always weak, the Mach number of the TWs is close to unity. Therefore, the UF TWs of the PODW are swept downstream in this case. Figure 7 shows the  $x$ -coordinates of the UF TWs identified in Fig. 6c over the period 497 to 545  $\mu\text{s}$ . It is observed that all these UF TWs are swept downstream.

In the EW, because of the decrease of the angle of the PODW, the post-shock tangential velocity increases. Consequently, as shown in Figs. 6c and 7, the downstream movement of the UF TWs accelerates, and the spacings between the UF TWs increase. According to our numerical results, there are some new UF TWs formed between the

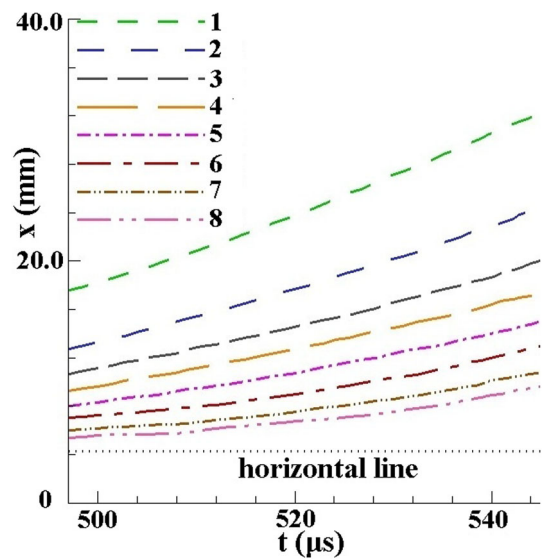
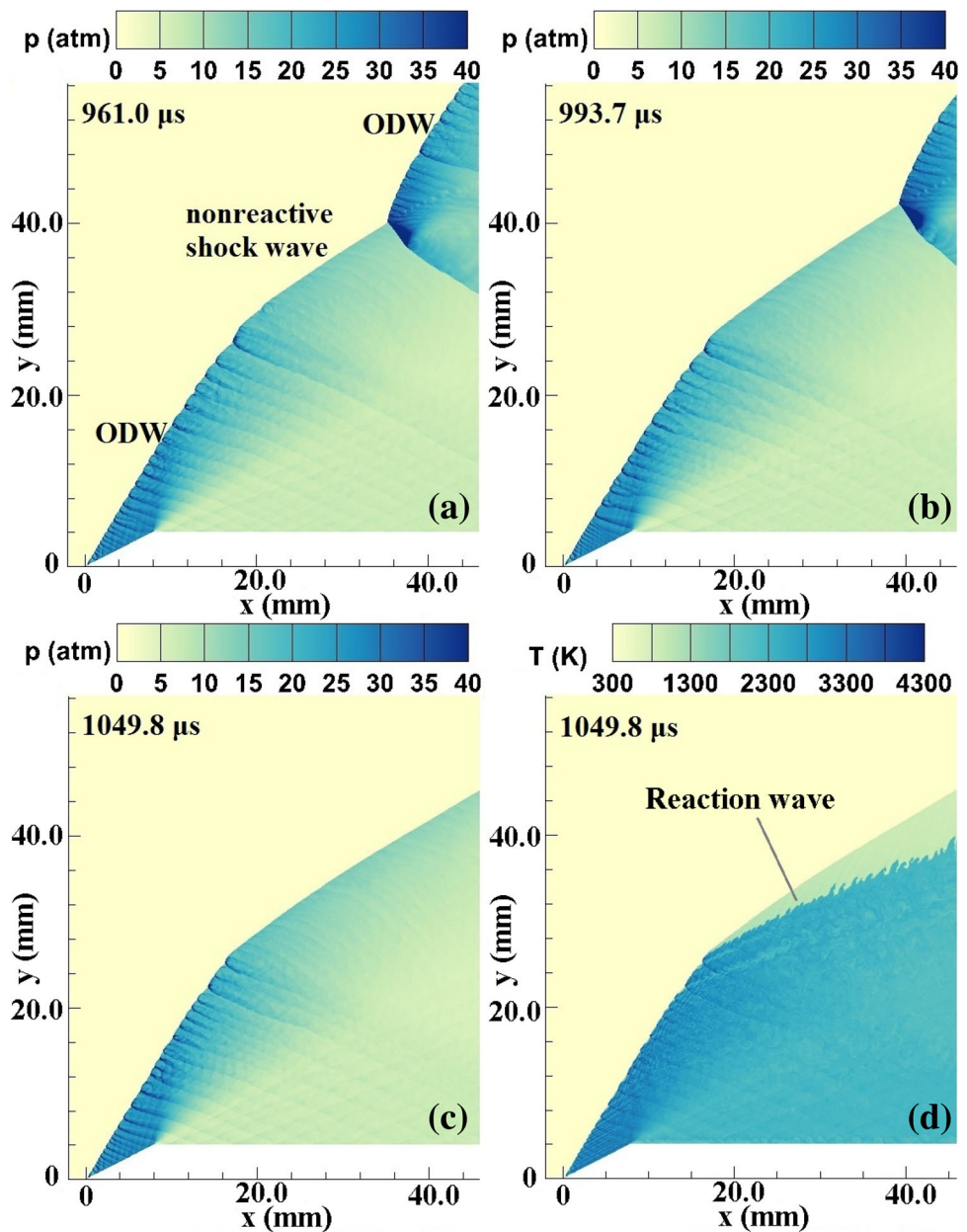


**Fig. 7**  $x$ -coordinates of the UF TWs identified in Fig. 6c

old ones. However, the newly formed UF TWs are scarce and weak, and their influence on the wave front is weak. Because of the large spacings between the UF TWs, the detonation wave front becomes somewhat irregular. According to the experimental results of Radulescu and Lee [27], for an irregular detonation, TW interactions are essential to its sustenance. Therefore, the TWs from upstream are essential in sustaining the detonation wave. The formation of a fully coupled PODW in this case should result from the downstream propagating UF TWs. According to the experiments near criticality of Maeda et al. [28], more new TWs will be formed as the PODW moves downstream. They will play an important role in sustaining the detonation wave. The PODW will become self-sustainable as it moves downstream.

**Fig. 8** Formation process of the partially coupled PODW at  $M = 6.5$  and  $l_w = 9$  mm



### 3.2.3 Partially coupled PODW

As shown in Fig. 8, an ODW is successfully formed above the wedge at  $M = 6.5$  and  $l_w = 9$  mm. The length of the induction region  $l_{\text{num,ind}}$  is less than 1 mm, which is much shorter than  $l_{\text{p-s,ind}}$ , 17.4 mm. Therefore, this ODW is a PODW. However, this PODW decouples eventually. As shown in Fig. 8a, the decoupled non-reactive shock wave is followed by another ODW. This configuration is named as the straw-hat type by Kasahara et al. [18–21]. The formation of the second ODW results from the coalescence of the initiated locations in the flow downstream of the PODW. These initiated locations are formed during the initiation process or the destabilization process of the PODW.

Therefore, the second ODW appears both in the initiation process and the below-mentioned re-stabilization process of the PODW. As noted in Fig. 8a–c, the second ODW is convected downstream. Similar phenomena have also been observed in the experiments of Maeda et al. [22]. Figure 8d shows the temperature field of the PODW in Fig. 8c. As shown in Fig. 8d, the detonation products and the shocked mixtures of the non-reactive shock wave are separated by a reaction wave.

As noted in Fig. 8, the PODW is weakened by the EW emanating from the corner. The angle of the PODW above the wedge is about  $58^\circ$ , which compares well with the shock polar analysis result,  $58.3^\circ$ . The corresponding normal Mach number of the PODW is about 5.5, which is greater than  $M_{CJ}$ , 4.84. Therefore, the PODW is overdriven with  $f = 1.3$ . The angle of the PODW at the decoupling point is about  $53^\circ$ . The corresponding normal Mach number is about 5.19, which is greater than  $M_{CJ}$ , 4.84. Therefore, the decoupling occurs before the PODW is attenuated to a CJ ODW. According to the shock polar analysis, the post-shock tangential Mach numbers of the PODW above the wedge and at the decoupling point are 1.06 and 1.26, respectively. Figure 9 shows the evolution process of the TWs of the PODW at  $M = 6.5$  and  $l_w = 9$  mm. Two UF TWs are identified in Fig. 9a, b. A comparison of these two UF TWs shows that they propagate upstream. The upstream propagation of the UF TWs may result from the low post-shock tangential Mach number of the PODW. As a result, the UF TWs cannot initiate combustion in the flow downstream of the non-reactive shock wave.

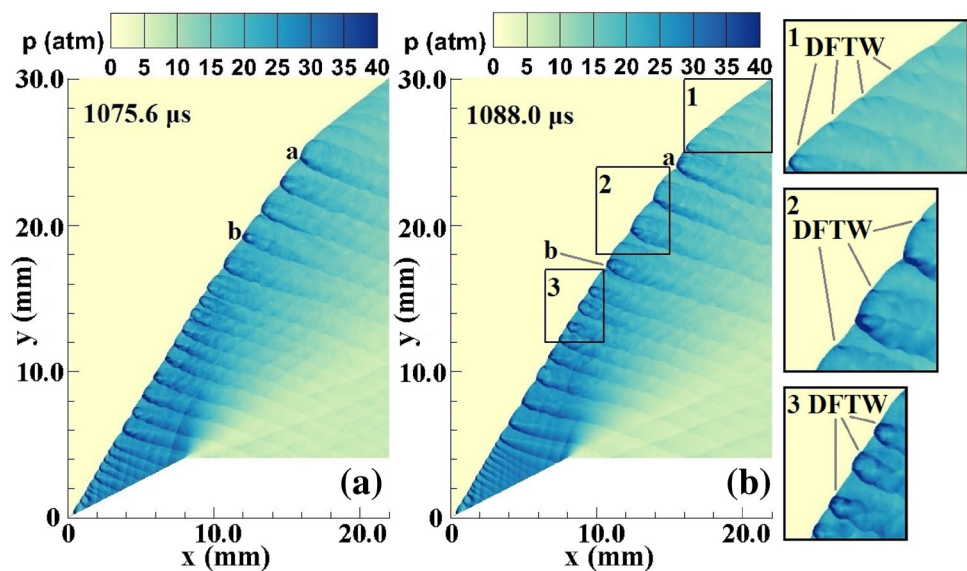
As mentioned above, the PODW is weakened by the EW. For the DF TWs, their post-shock temperature and pressure are decreased, and consequently their post-shock reaction process is slowed down. As a result, the DF TWs become

weaker and weaker as they propagate through the EW. To investigate the evolution process of the DF TWs, three close-up views of Fig. 9b are shown and numbered as 1–3. It is observed in the close-up views that the DF TWs become weaker and weaker as they propagate downstream. Moreover, as observed in the close-up view numbered 1, the DF TWs become so weak that they cannot initiate combustion in the flow downstream of the non-reactive shock wave. In summary, both the UF TWs and the DF TWs cannot initiate combustion in the flow downstream of the non-reactive shock wave in this case. Therefore, this case results in a partially coupled PODW.

As observed in Fig. 8d, the detonation products and the shocked mixtures are separated by a reaction wave. The shape of the reaction wave is irregular. Many projections comprised of burned mixtures are formed on the reaction wave. A similar phenomenon has also been observed in the experiments of Verreault and Higgins [4], Kasahara et al. [19, 20], and Maeda et al. [22]. We traced the evolution process of these projections. Figure 10 shows the evolution process of one projection. It is observed that the projection is formed by the passage of a weakened DF TW, as shown in Fig. 10a. Then the projection grows as it is convected downstream as observed in Fig. 10b, c. The same phenomena have also been observed for the other projections. Further, similar phenomena have also been observed in the numerical results of Jones et al. [29] for detonation re-initiation in area expansions.

As shown in Fig. 11a, b, a shock wave resulting from local explosion is observed to occur in the shocked mixture above the reaction wave. A similar phenomenon has also been observed in the experiments of Maeda et al. [22]. Resulting from the local explosion, the shocked mixtures are all initiated, and a fully coupled PODW is formed as shown

**Fig. 9** Evolution process of the transverse waves of the PODW at  $M = 6.5$  and  $l_w = 9$  mm



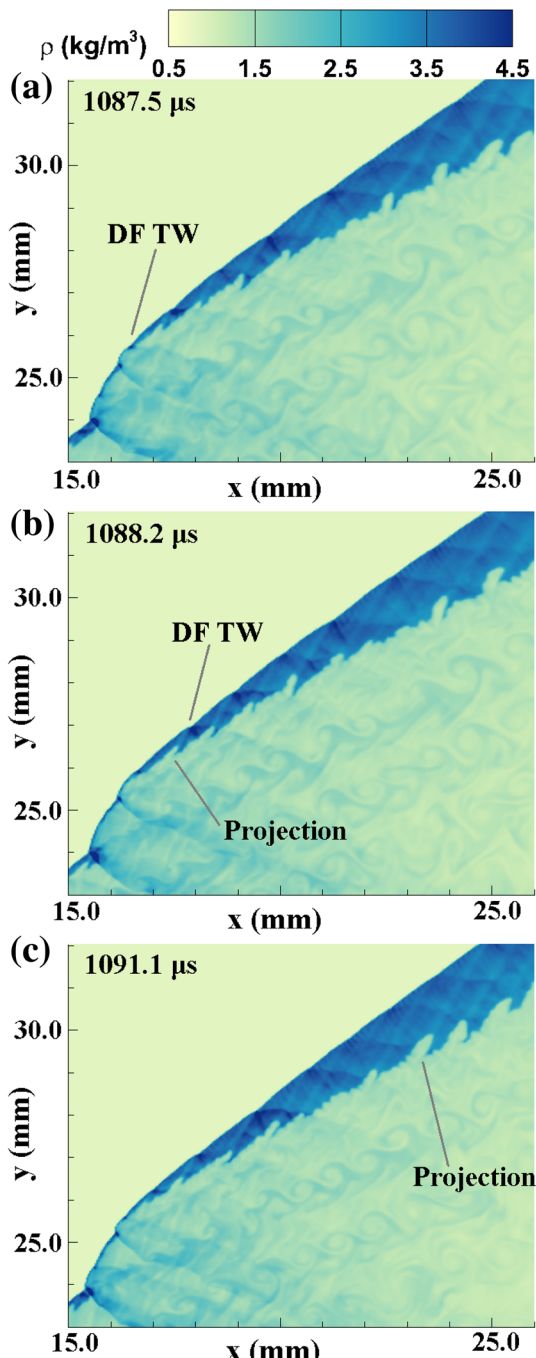


**Fig. 10** Evolution process of the projections on the reaction wave at  $M = 6.5$  and  $l_w = 9$  mm

in Fig. 11c. The wave angle of the fully coupled PODW decreases under the weakening effect of the EW and reaches a constant value eventually. The normal Mach number of the weakened PODW is about 4.9, which compares well with  $M_{CJ}$ , 4.84. Therefore, the PODW behind the EW should be at the CJ state. However, this fully coupled PODW cannot persist for long. The fully coupled PODW decays gradually, and a new partially coupled PODW is eventually formed as

shown in Fig. 11d. The destabilization process of the partially coupled PODW as shown in Fig. 11 occurred twice in the numerical simulation, at  $M = 6.5$  and  $l_w = 9$  mm. The disturbed PODWs both re-stabilized to a partially coupled PODW.

To investigate the influence of the wedge length on the partially coupled PODW, the numerical simulations with  $l_w = 5$  and 7 mm were performed. Figure 12 shows the corresponding pressure fields of the partially coupled PODWs. At  $l_w = 5$  and 7 mm, the angles of the PODWs at the decoupling points are about  $55^\circ$  and  $54^\circ$ , respectively. The corresponding normal Mach numbers are about 5.32 and 5.26, respectively. They both are greater than  $M_{CJ}$ , 4.84. Therefore, the PODWs are both overdriven when decoupling occurs. A similar phenomenon has also been observed at  $l_w = 9$  mm. The height of the PODW  $h_{PODW}$  is observed to increase with the wedge length. The height of the PODW at  $l_w = 5$  mm is about 10.8 mm, and it is smaller than the height of the PODW at  $l_w = 7$  mm, which is 22.0 mm. The height of the PODW at  $l_w = 9$  mm, which is more than 25.0 mm, is greater than that at  $l_w = 7$  mm. Furthermore, the local explosion that occurred above the reaction wave at  $l_w = 9$  mm also occurred in the cases of  $l_w = 5$  and 7 mm. It can be concluded that the stability of the partially coupled PODW is weak. The configuration of the partially coupled PODW can be altered by local explosions occurring above the reaction wave. Even though we observed local explosions several times in our numerical results, the mechanism for the formation of such a local explosion is still unclear. Further research on the mechanism of the formation of the local explosion is still needed.

#### 4 Conclusions

The PODW sustained by a finite-length wedge is investigated by numerical simulation.

1. The numerical results show that it is possible to stabilize a PODW on a finite-length wedge shorter than the induction length of the mixture behind the inert shock by numerically imposing a premature initiation of combustion in the initial flow field.
2. The fully coupled and the partially coupled PODWs are observed in the numerical results. For the fully coupled PODW, the UF TWs are swept downstream and consequently a fully coupled PODW can persist.
3. For the partially coupled PODW, the UF TWs propagate upstream, and the DF TWs are weakened by the EW. Neither TWs can initiate combustion in the flow downstream of the non-reactive shock wave, resulting in a partially coupled PODW. The stability of the partially coupled PODW is weak. The configuration of the partially coupled PODW is observed to be destabilized by

**Fig. 11** Destabilization process of the partially coupled PODW at  $M = 6.5$  and  $l_w = 9\text{ mm}$

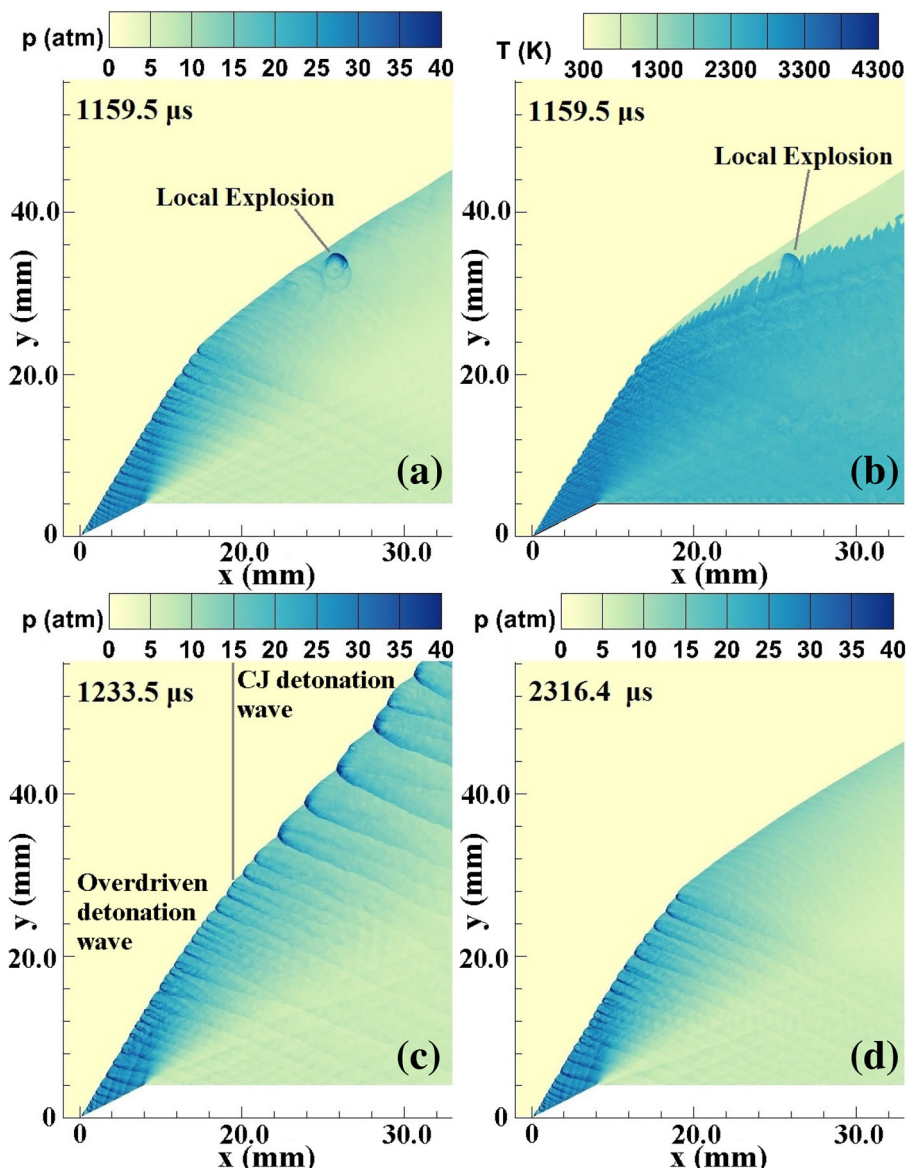
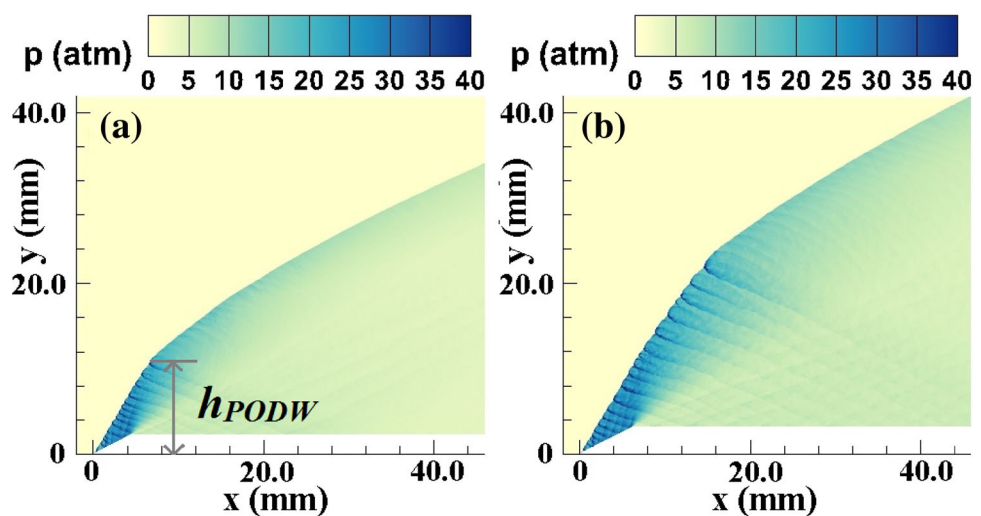


**Fig. 12** Pressure fields of the PODWs at  $M = 6.5$ ,  $l_w = \mathbf{a}$  5 mm and  $\mathbf{b}$  7 mm



local explosions occurring above the reaction wave in the cases of  $M = 6.5$  and  $l_w = 5, 7$ , and 9 mm.

**Acknowledgments** This work was sponsored by the National Natural Science Foundation of China (No. 91441110).

## References

1. Ashford, S.A., Emanuel, G.: Oblique detonation wave engine performance prediction. *J. Propuls. Power* **12**(2), 322–327 (1996)
2. Hertzberg, A., Bruckner, A.P., Bogdanoff, D.W.: Ram accelerator: a new chemical method for accelerating projectile to ultrahigh velocities. *AIAA J.* **26**(2), 195–203 (1988)
3. Figueira da Silva, L.F., Deshaies, B.: Stabilization of an oblique detonation wave by a wedge: a parametric numerical study. *Combust. Flame* **121**, 152–166 (2000)
4. Verreault, J., Higgins, A.J.: Initiation of detonation by conical projectiles. *Proc. Combust. Inst.* **33**, 2311–2318 (2011)
5. Lefebvre, M.H., Fujiwara, T.: Numerical modeling of combustion processes induced by a supersonic conical blunt body. *Combust. Flame* **100**, 85–93 (1995)
6. Liu, Y., Dan, W., Yao, S.-B., Wang, J.-P.: Analytical and numerical investigations of wedge-induced oblique detonation waves at low inflow Mach number. *Combust. Sci. Tech.* **187**(6), 843–856 (2015)
7. Li, C., Kailasanath, K., Oran, E.S.: Detonation structures behind oblique shocks. *Phys. Fluids* **6**, 1600–1611 (1994)
8. Liu, Y., Liu, Y.S., Wu, D., Wang, J.P.: Structure of an oblique detonation wave induced by a wedge. *Shock Waves* (2016). doi:[10.1007/s00193-015-0600-5](https://doi.org/10.1007/s00193-015-0600-5) (in press)
9. Papalexandris, M.V.: A numerical study of wedge-induced detonations. *Combust. Flame* **120**, 526–538 (2000)
10. Teng, H.-H., Jiang, Z.-L.: On the transition pattern of the oblique detonation structure. *J. Fluid Mech.* **713**, 659–669 (2012)
11. Teng, H.-H., Jiang, Z.-L., Ng, H.D.: Numerical study on unstable surfaces of oblique detonations. *J. Fluid Mech.* **744**, 111–128 (2014)
12. Choi, J.-Y., Kim, D.-W., Jeung, I.-S., Ma, F., Yang, V.: Cell-like structure of unstable oblique detonation wave from high-resolution numerical simulation. *Proc. Combust. Inst.* **31**(2), 2473–2480 (2007)
13. Teng, H.-H., Ng, H.D., Li, K., Luo, C.-T., Jiang, Z.-L.: Evolution of cellular structures on oblique detonation surfaces. *Combust. Flame* **162**, 470–477 (2015)
14. Verreault, J., Higgins, A.J., Stowe, R.A.: Formation of transverse waves in oblique detonations. *Proc. Combust. Inst.* **34**(2), 1913–1920 (2013)
15. Gui, M.-Y., Fan, B.-C., Dong, G.: Periodic oscillation and fine structure of wedge-induced oblique detonation waves. *Acta Mech. Sin.* **27**, 922–928 (2011)
16. Walter, M.A.T., Figueira da Silva, L.F.: Numerical study of detonation stabilization by finite length wedges. *AIAA J.* **44**(2), 353–361 (2006)
17. Pimentel, C.A.R., Azevedo, J.L.F., Figueira da Silva, L.F.: Numerical study of wedge supported oblique shock wave-oblique detonation wave transitions. *J. Braz. Soc. Mechan. Sci.* **XXIV**, 149–157 (2002)
18. Kasahara, J., Takeishi, A., Kuroda, H., Horiba, M., Matsukawa, K., Leblanc, J.E., Endo, T., Fujiwara, T.: Experimental observation of oblique detonation waves around hypersonic free projectiles. In: Takayama, K., Sasoh, A. (eds.) *Ram Accelerators*, pp. 263–270. Springer-Verlag, Heidelberg, Germany (1998)
19. Kasahara, J., Arai, T., Chiba, S., Takazawa, K., Tanahashi, Y., Matsuo, A.: Criticality for stabilized oblique detonation waves around spherical bodies in acetylene/oxygen/krypton mixtures. *Proc. Combust. Inst.* **29**, 2817–2824 (2002)
20. Kasahara, J., Fujiwara, T., Endo, T., Arai, T.: Chapman-Jouguet oblique detonation structure around hypersonic projectiles. *AIAA J.* **39**, 1553–1561 (2001)
21. Kasahara, J., Arai, T., Matsuo, A., Akai, N., Takazawa, K.: Experimental investigation of steady-state oblique detonation waves generated around hypersonic projectiles. *AIAA-2001-1800*
22. Maeda, S., Inada, R., Kasahara, J., Matsuo, A.: Visualization of the non-steady state oblique detonation wave phenomena around hypersonic spherical projectile. *Proc. Combust. Inst.* **33**, 2343–2349 (2011)
23. Korobeinikov, V.P., Levin, V.A., Markov, V.V., Chernyi, G.G.: Propagation of blast waves in a combustible gas. *Astronaut. Acta* **17**(4–5), 529–537 (1972)
24. Liu, Y.-F.: *Numerical Studies on Detonation and Pulse Detonation Engines* (in Chinese). College of Engineering, Peking University, Beijing (2004)
25. Steger, J.L., Warming, R.F.: Flux vector splitting of the inviscid gasdynamic equations with application to finite-difference methods. *J. Comput. Phys.* **40**(2), 263–293 (1981)
26. Balsara, D.S., Shu, C.-W.: Monotonicity preserving weighted essentially non-oscillatory schemes with increasingly high order of accuracy. *J. Comput. Phys.* **160**(2), 405–452 (2000)
27. Radulescu, M.I., Lee, J.H.S.: The failure mechanism of gaseous detonations: experiments in porous wall tubes. *Combust. Flame* **131**, 29–46 (2002)
28. Maeda, S., Sumiya, S., Kasahara, J., Matsuo, A.: Initiation and sustaining mechanisms of stabilized oblique detonation waves around projectiles. *Proc. Combust. Inst.* **34**, 1973–1980 (2013)
29. Jones, D.A., Kemister, G., Tonello, N.A., Oran, E.S., Sichel, M.: Numerical simulation of detonation reignition in  $H_2-O_2$  mixtures in area expansions. *Shock Waves* **10**, 33–41 (2000)